International Journal of Energy Research

INTERNATIONAL JOURNAL OF ENERGY RESEARCH
Int. J. Energy Res. 2013; **37**:1475–1487
Published online 15 November 2012 in Wiley Online Library (wileyonlinelibrary.com). DOI: 10.1002/er.2955

A dimensionless numerical analysis for the optimization of an active magnetic regenerative refrigerant cycle

C. Aprea[1], A. Greco[2,*,†] and A. Maiorino[1]

[1]Dipartimento di Ingegneria Meccanica, Università di Salerno, via Ponte Don Melillo, 84084 Fisciano, Salerno, Italia
[2]DETEC, Università degli Studi di Napoli Federico II, P.le Tecchio 80, 80125 Napoli, Italia

SUMMARY

Refrigeration by an active magnetic regenerative system (AMR) is potentially more attractive, as compared to conventional techniques. Indeed, devices based upon an AMR cycle are more efficient, compact, environment-friendly and can operate over a broad range of temperatures. In this paper, attention is focused to the near room-temperature range.

On the other hand, however, the AMR cycle poses a variety of complex problems, in terms of fluid dynamics, heat transfer and magnetic field. In order to identify the optimal operational parameters, the design and optimization of a magnetic refrigeration system can be supported by modelling. In this paper, a dimensionless approach was adopted to simulate an AMR cycle following a Brayton regenerative cycle. In the simulation, the temperature range that has been explored is 260 – 280 K and 275 – 295 K. The heat transfer mediums are, respectively, water–glycol mixture (50% by weight) and pure water. The $Gd_{0.8}Dy_{0.2}$ alloy and pure Gd have been chosen as constituent material for the regenerator of the AMR cycle. With this model, the influence of the different parameters on cycle efficiency has been analysed. In particular, the study has been focused on the influence of the secondary fluid properties, magnetic material particle diameter, fluid blow time, secondary fluid mass flow rate, regenerator geometry and effect of axial thermal conduction. The model enables to find optimal dimensionless numbers in order to maximize the cycle performances. The results can be extended to widely different situations and therefore can be easily employed for the design and the optimization of new experimental prototypes. Copyright © 2012 John Wiley & Sons, Ltd.

KEY WORDS

magnetic refrigeration; active magnetic regenerative refrigerant cycle; second law coefficient of performance; dimensionless analysis; operating parameters

Correspondence

*A. Greco, DETEC, Università degli Studi di Napoli Federico II, P.le Tecchio 80, 80125, Italia.
†E-mail: adriana.greco@unina.it

Received 16 January 2012; Revised 6 July 2012; Accepted 4 August 2012

1. INTRODUCTION

Magnetic refrigeration is an innovative technology based on the magnetocaloric effect (MCE) in solid-state refrigerants [1,2]. In the case of ferromagnetic materials, the MCE yields warming, as the magnetic moments of the atom are aligned by the magnetic field. Whereas the MCE yields cooling with the removal of the magnetic field. Therefore, MCE can be regarded as an adiabatic temperature change in a reversible process or, alternatively, as an isothermal magnetic temperature change. This property strongly depends on the intensity of the magnetic field and on the temperature, and it is maximized at the Curie temperature of the magnetic material.

Approximately 15% of the overall energy consumption in the world can be attributed to refrigeration processes [3–5]. Among them, air conditioning uses the greatest amounts of electric energy, and therefore, although indirectly, it is the major carbon dioxide producer.

Modern refrigeration is based on vapour compression plants. This technology is mature and only marginal efficiency improvements can be expected in the future. Furthermore, conventional systems use ozone-depleting and global-warming gases, thus producing further, undesirable environmental effects.

On the contrary, magnetic refrigeration is an intrinsically environment-friendly and energetically efficient technique. Indeed, the magnetic refrigerant is a solid, with essentially zero vapour pressure. Therefore, it is characterized by no ozone depletion potential and zero direct global warming potential [6].

The research in magnetic refrigeration is mainly focused on the improvement of magnetic materials, of cycle thermodynamics of fluid dynamics and on the development of an optimal design for prototype construction.

Recently, different experimental prototypes have been built and tested, most of them running in the near room-temperature range [7]. A review of the experimental

Copyright © 2012 John Wiley & Sons, Ltd.

prototypes is reported in [8,9]. Different mechanical realizations of the active magnetic regenerative (AMR) cycle have been tested. In many experimental devices, the magnetic field is generated by means of an electromagnet or of a superconducting electromagnet. Therefore, these configurations are not of practical interest and are applicable only in the cryogenic temperature range. In the room-temperature field are possible only devices with a permanent magnet to generate a magnetic field. Between the experimental prototypes developed, most of them have low cooling power and low energetic performances and therefore are not useful for practical applications. Attention should be paid on the development of a new experimental prototype characterized by a greater cooling power and energetic performances better than those of a traditional vapour compression plant for commercial applications. To this aim, further technological developments are still required. Construction and experimental optimization of a prototype magnetic refrigeration system are costly and time-consuming. Therefore, at least initially, fruitful results in terms of optimal operational parameter identification can be obtained by theoretical modelling.

Different analytical models have been developed in order to evaluate the potential of an AMR cycle; a review of them is reported in [10]. Most of them are mono-dimensional, but two- and three-dimensional models have been also presented. For 2D and 3D models, the computation time may be prohibitive, and the possibility of varying the regenerator geometry is limited. A comparison between the 1D and 2D models show excellent agreement for packed sphere regenerators and for flat parallel plates regenerators with thin regenerator channels [11].

All the presented models are in dimensional form, and therefore the results are applicable only to the operating conditions analysed. In order to generalize the results, a dimensionless numerical number has been developed in the present paper. Based on this model, the influence of the different dimensionless numbers on cycle efficiency has been analysed.

2. THE AMR CYCLE

In an AMR refrigerationcycle, instead of using a separate material as a regenerator to recuperate the heat from the magnetic material, the magnetic material matrix works both as a refrigerating medium and as a heat regenerating medium. The magnetic material is magnetized increasing its temperature and then demagnetized decreasing its temperature. Since the refrigerant is a solid, for example in the shape of spherical particles, the heat transfer must be facilitated by a secondary fluid flowing through the regenerator. The secondary fluid can be a liquid (e.g. water or aqueous anti-freeze solutions) or a gas (e.g. helium, nitrogen and carbon dioxide).

The magnetic field of magnetic refrigeration cycle can be supplied by electromagnet, superconductor or permanent magnet.

An electromagnet generates a magnetic flux density by passing a current through a solenoid. Although an electromagnet can create magnetic flux density of 10 T, this is not a commercial solution because it needs a great power supply. A superconducting magnet is a better option because it requires little power to operate once the electromagnet has become supeconducting as no power is lost for ohmic resistance. Although a supeconducting magnet can create magnetic flux density of the order of 15–20 T, it has to be continuously cooled. This can be an expensive process, and the apparatus surrounding the supeconducting magnet can be substantial. However, for large-scale central cooling systems (e.g. large refrigerators for warehouses), a superconducting magnet might be a relevant solution. For commercial household refrigeration, the superconducting magnet is at present not a relevant solution because the power required by cryogenic equipment necessary to maintain the superconducting temperature of a solenoid magnet can greatly exceed the cooling power.

Therefore, commercial household refrigeration practical application use permanent magnets to produce the magnetic field [12,13]. The magnetic flux generated by a permanent magnet cannot exceed, for a NdFeB in Halbach configuration, 1.4 – 1.5 T [14–17]

For the magnetic material, there are two types of magnetic phase changes that may occur at the Curie point: first-order magnetic transition and second-order magnetic transition. The first-order materials exhibit a giant MCE, but three major problems arise in their use: (i) in a first-order magneto structural transition, a large volume change occurs; (ii) large hysteresis; and (iii) a finite time for the adiabatic temperature variation to reach its maximum equilibrium value. Therefore, in this paper attention is paid on second-order materials with the Curie temperature in the room-temperature range.

Gadolinium, a member of the lanthanide group of elements, is a typical magnetic material in this temperature range. At the Curie temperature T_C of 294 K, Gd undergoes a second-order paramagnetic – ferromagnetic phase transition. Pure gadolinium regenerator exhibits a large MCE only over a small temperature range containing its Curie temperature. A variety of Gd – R alloys, where R is another lanthanide metal (Tb, Dy, Ho or Er), can be prepared [18–20]. Using alloys as constituent material of the regenerator, it is possible to vary the Curie temperature varying the composition. Therefore, for each temperature span, it is possible to select the correct composition in order to reach the maximum MCE.

Figure 1 shows a schematic of a typical AMR device, which consists primarily of: (i) an AMR bed made of solid magnetic material (in a shape of packed bed in most cases); (ii) a permanent magnet to generate the magnetic field; (iii) a circulating fluid (water or water/anti-freeze mixture); (iv) a variable speed pump for flow circulation; (v) a group of valve for the direction of the fluid flow through the regenerator; (vi) a cold heat exchanger; (vii) a hot heat exchanger.

An AMR cycle [21] consists of the four following processes: (i) bed magnetization; (ii) iso-field cooling; (iii) bed demagnetization; (iv) iso-field heating.

In the magnetization process, the magnetic field in the bed is applied with no fluid flow. Then, the temperature of the magnetic material rises due to the MCE.

Int. J. Energy Res. 2013; **37**:1475–1487 © 2012 John Wiley & Sons, Ltd.
DOI: 10.1002/er

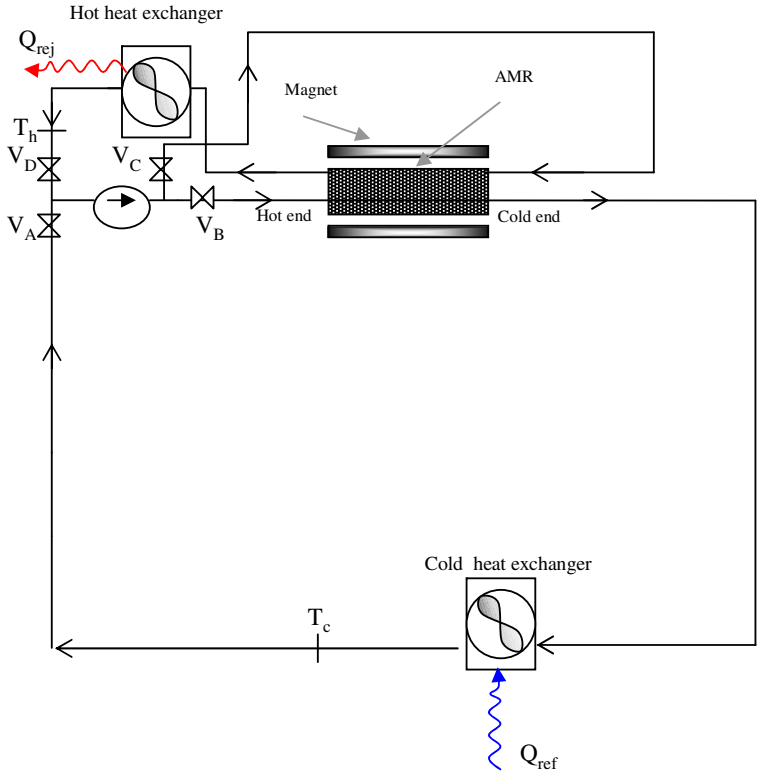

Figure 1. A schematic view of an AMR cycle.

In the iso-field cooling process, the heat transfer fluid is blown from the cold end to the hot end of the bed while maintaining the applied field. In this process, the temperature of the fluid is lower than that of the bed; thus, the magnetic material temperature decreases because the fluid absorbs heat from the bed. In this process, valves V_D and V_B are open, and valves V_A and V_C are closed. The secondary fluid at a temperature higher than T_h enters in the hot heat exchanger, expels heat (Q_{rej}) and is cooled to the temperature T_h.

In the demagnetization process, magnetic field is removed, and thus the magnetic material temperature decreases with no fluid flow.

Finally, in the iso-field heating, with a zero field, the fluid is blown from the hot end to the cold end of the bed. In this process, the temperature of the fluid is higher than that of the bed, therefore the magnetic material temperature increases, and the secondary fluid temperature decreases to a temperature lower than T_c. In this process, valves V_A and V_C are open, and valves V_D and V_B are closed. The secondary fluid enters in the cold heat exchanger, rejects heat producing the cooling load (Q_{ref}) and is heated to the temperature T_c, and the cycle is repeated.

3. MODELLING OF AMR CYCLE

In order to analyse and design an optimum magnetic refrigeration system, it is important to model the magnetization and demagnetization process of the magnetic material and the regenerative warm and cold blow processes. The initial and the boundary conditions of each process connect each step of the four sequential processes to allow a cyclical operation of the AMR system [22–25].

The regenerator bed in this simulation has the shape of a packed bed made of spheres of constant diameter.

In this study, a 1D unsteady model has been proposed. This model takes into account most of the physical problems of an AMR cycle, namely:

- axial conduction in the solid and in the fluid;
- the viscous dissipation due to the fluid flow throughout the regenerator;
- the dependence of the magnetic material properties on temperature and on applied magnetic field (for example specific heat Cs);
- the dependence of the secondary fluid properties on temperature.

The following simplifying assumptions have been adopted:

- the temperature of the secondary fluid entering at each end of the refrigerant bed is constant;
- the bed is assumed adiabatic towards the environment;
- the magnetic material is isotropic;
- the fluid flow through the bed is parallel and uniform throughout any cross section. The temperature change perpendicular to the main flow direction can be

therefore neglected, and the problem can be considered one dimensional;
- the regenerator surface area is evenly distributed throughout its volume;
- the solid spheres are of uniform shape and incompressible.

Based on the above assumptions, an energy balance for the secondary fluid and for the magnetic material can be performed [26–29] and the following equations in general form can be obtained:

$$\begin{cases} \mathrm{m_f\ c_f}\ \dfrac{\partial \mathrm{T_f}}{\partial \mathrm{t}} + \dot{\mathrm{m}}_\mathrm{f}\ \mathrm{L}\ \mathrm{c_f}\dfrac{\partial \mathrm{T_f}}{\partial \mathrm{x}} - (A.K.)_f = \mathrm{h}\ \mathrm{A_{SC}}\ (\mathrm{T_s} - \mathrm{T_f}) + \left(\dfrac{\partial \mathrm{p}}{\partial x}\right)\dfrac{\dot{m}_f}{\rho_f}L \\ \mathrm{m_s\ c_s}\dfrac{\partial \mathrm{T_s}}{\partial \mathrm{t}} - (A.K.)_s = \mathrm{h}\ \mathrm{A_{SC}}\ (\mathrm{T_f} - \mathrm{T_s})\text{-}\mathrm{m_s}T_s\left(\dfrac{\partial s_s}{\partial H}\right)_T\left(\dfrac{\partial H}{\partial t}\right) \end{cases} \quad (1)$$

In equation (1), the terms $(\mathrm{A.K.})_\mathrm{f}$ and $(\mathrm{A.K.})_\mathrm{s}$ represent the axial conduction in the fluid and solid equation, respectively. These terms assume different form in the different models reported.

The surface area of the packed bed which appears in both energy equations is developed based on geometrical considerations and is defined as:

$$A_{sc} = \frac{6}{d_p}V(1-\varepsilon) \quad (2)$$

The fluid-to-solid heat transfer coefficient in this study is based on the Wakao *et al*. [30,31] empirical correlation:

$$h = \frac{k_f}{d_p}\left[2 + 1.1\ \mathrm{Pr}_\mathrm{f}^{1/3}\mathrm{Re}_f^{0.6}\right] \quad (3)$$

The Ergun equation [32] is used for the pressure drop in secondary fluid flow:

$$\frac{\partial p}{\partial x} = 180\left(\frac{1-\varepsilon}{\varepsilon}\right)^2\frac{\mu_f}{d_p}w_{\mathrm{inf}} + 1.8\left(\frac{1-\varepsilon}{\varepsilon^2}\right)\frac{\rho_f}{d_p}w_{\mathrm{inf}}^2 \quad (4)$$

where $\mathrm{w_{inf}}$ is evaluated as: $w_{\mathrm{inf}} = \frac{\dot{\mathrm{m}}_\mathrm{f}}{\rho_\mathrm{f}\mathrm{A}}$

Both equations (1) can be written in dimensionless form with the introduction of the following dimensionless temperature, length, time and magnetic field [33]:

$$\vartheta = \frac{T - T_c}{T_h - T_c};\quad \mathrm{x^*} = \frac{x}{L};\quad \mathrm{t^*} = \frac{t}{\tau};\quad \mathrm{H^*} = \frac{H - H_{\mathrm{min}}}{H_{\mathrm{max}} - H_{\mathrm{min}}} \quad (5)$$

The equations in dimensionless form are:

$$\begin{cases} \dfrac{\partial \vartheta_\mathrm{f}}{\partial \mathrm{x^*}} + \dfrac{\partial \vartheta_\mathrm{f}}{\partial \mathrm{t^*}} - (\mathrm{A.K.})_{\mathrm{f,dl}} = \mathrm{NTU}\ (\vartheta_\mathrm{s} - \vartheta_\mathrm{f}) + \left(\dfrac{\partial \mathrm{p^*}}{\partial \mathrm{x^*}}\right) \\ \dfrac{\partial \vartheta_\mathrm{s}}{\partial \mathrm{t^*}} - (\mathrm{A.K.})_{\mathrm{s,dl}} = \Phi\mathrm{NTU}\left(\vartheta_\mathrm{f} - \vartheta_\mathrm{s}\right)\text{-}S_\mathrm{H}\left(\dfrac{\partial \mathrm{H^*}}{\partial \mathrm{t^*}}\right) \end{cases} \quad (6)$$

In equation (6), the terms $(\mathrm{A.K.})_{\mathrm{f,dl}}$ and $(\mathrm{A.K.})_{\mathrm{s,dl}}$ represent the dimensionless axial conduction terms in the fluid and solid equation, respectively.

The following dimensionless numbers have been used:

- NTU – number of heat transfer units:

$$NTU = \frac{hA_{SC}}{\dot{m}_f C_f} \quad (7)$$

- Φ – utilization factor:

$$\Phi = \frac{\dot{\mathrm{m}}_\mathrm{f}\mathrm{C_f P}}{\mathrm{m_s C_s}} \quad (8)$$

in this equation, P is the secondary fluid flow blow time ($\mathrm{t_{HF}} = \mathrm{t_{CF}}$). This dimensionless number is fundamental in the design of a prototype because it represents the ratio of the thermal mass of the secondary fluid to the total thermal mass of the solid regenerator.

- p* – dimensionless pressure:

$$\mathrm{p^*} = \frac{\mathrm{p}}{\rho_\mathrm{f}\mathrm{C_f}(\mathrm{T_h}\text{-}\mathrm{T_c})} \quad (9)$$

- $\mathrm{S_H}$ – dimensionless number characterizing the magnetic material, defined as:

$$S_H = \frac{\left(\frac{\partial s_s}{\partial H^*}\right)_{\vartheta_s}}{\left(\frac{\partial s_s}{\partial \vartheta_s}\right)_{H^*}} \quad (10)$$

The mean field theory describes the thermodynamic properties of a ferromagnetic material and can be used to calculate the magnetocaloric properties of gadolinium and of gadolinium-based alloy [34–39].

Comparing the numerical results for Gd and Gd–Dy alloy obtained with experimental results supplied by others, a good compromise has been found.

To solve the resulting mathematical method, a computer program has been developed. The solution of both equations requires boundary and initial conditions connecting each process of the cycle.

A flow chart of the program is reported in Figure 2.

3.1. Model with no axial conduction (model 1)

In this model, the axial conduction is neglected. Therefore:

$$(\mathrm{A.K.})\mathrm{f} = (\mathrm{A.K.})\mathrm{s} = 0 \quad (11)$$

Int. J. Energy Res. 2013; **37**:1475–1487 © 2012 John Wiley & Sons, Ltd.
DOI: 10.1002/er

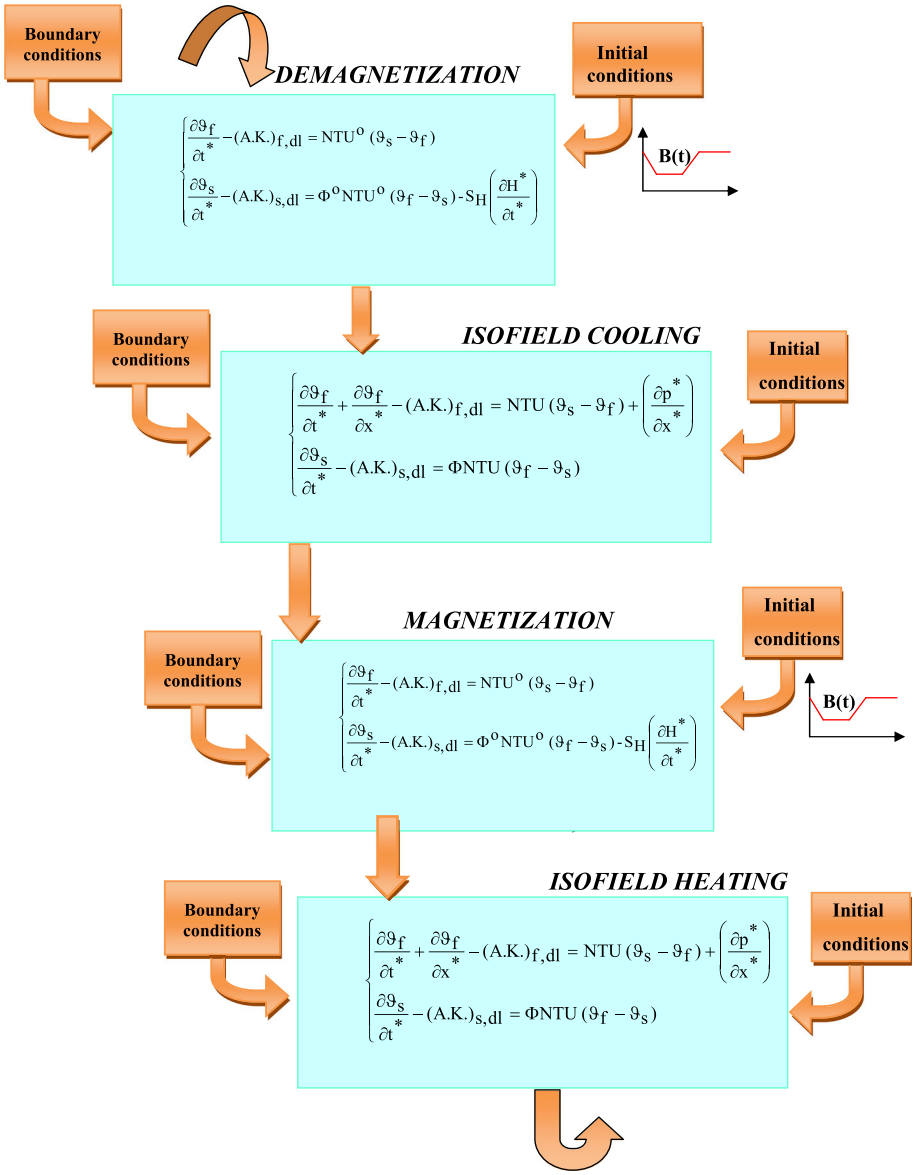

Figure 2. The flow chart of the computer program.

During demagnetization and magnetization phase, there is no fluid flow; therefore, in equation (1), $\dot{m}_f = 0$. In the iso-field cooling, the fluid moves from the cold to the hot side of the regenerator: therefore, in equation (1), $\dot{m}_f = \dot{m}_0$, and the dimensionless boundary condition is:

$$\vartheta_f(t^*, 0) = 0 \tag{12}$$

In the iso-field heating, the fluid moves from the hot to the cold side of the regenerator: therefore, in equation (1), $\dot{m}_f = -\dot{m}_0$, and the dimensionless boundary condition is:

$$\vartheta_f(t^*, 1) = 1 \tag{13}$$

3.2. Model with axial conduction in the solid equation (model 2)

In this model, the axial conduction is ignored in the fluid equation and instead is applied to the matrix and modelled using the concept of effective bed conductivity:

$$\begin{aligned} (A.K.)_f &= 0 \\ (A.K.)_s &= A\ L\ K_{eff,s}\ \frac{\partial^2 T_s}{\partial x^2} \end{aligned} \tag{14}$$

In this case, dispersion in the regenerator acts to mix fluid along the bed in the direction of flow and can be treated as an axial conduction term. Therefore, the total axial conductivity of a regenerator bed is a function of static effective thermal

conductivity and of fluid dispersion. The effective thermal conductivity can be evaluated as:

$$K_{eff,s} = k_{static} + k_f D_t{}^d \tag{15}$$

where k_{static} is the effective conductivity of the regenerator bed when there is no flow and can be evaluated with the Hadley correlation [40]:

$$k_{static} = k_f \left[(1-\alpha o) \frac{\varepsilon \cdot fo + \left(k_s/k_f\right)(1-\varepsilon \cdot fo)}{1-\varepsilon(1-fo) + \left(k_s/k_f\right)\cdot\varepsilon\cdot(1-fo)} + \alpha o \frac{2\left(k_s/k_f\right)^2(1-\varepsilon) + (1+2\varepsilon)\cdot k_s/_{k_f}}{(2+\varepsilon)\cdot k_s/k_f + 1 - \varepsilon} \right] \tag{16}$$

where for $\varepsilon < 0.58$:

$$\begin{aligned} fo &= 0.8 + 0.1\varepsilon \qquad 0 \le \varepsilon \le 0.0827 \\ \log \alpha o &= -4.898\varepsilon \end{aligned} \tag{17}$$

$$\log \alpha o = -0.405 - 3.154(\varepsilon - 0.0827) \qquad 0.0827 \le \varepsilon \le 0.298 \tag{18}$$

$$\log \alpha o = -1.084 - 6.778(\varepsilon - 0.298) \qquad 0.298 \le \varepsilon \le 0.580 \tag{19}$$

Where k_s is the bed thermal conductivity and k_f is the secondary fluid thermal conductivity.

The second term in equation (15) takes into account the fluid dispersion and can be evaluated according to Kaviany [32] as:

$$D_t{}^d = \varepsilon \frac{3}{4} Pe_f \tag{20}$$

The axial conduction term in dimensionless form is:

$$(\mathrm{A.K.})_{s,dl} = \frac{\mathrm{St_f}}{\mathrm{Bi_{eff}}} \Phi \frac{\partial^2 \theta_s}{\partial x^{*2}} \tag{21}$$

Where the following dimensionless numbers have been used:

- $\mathrm{St_f}$ – fluid Stanton number:

$$\mathrm{St_f} = \frac{\mathrm{Nu}}{\mathrm{RePr}} \tag{22}$$

- $\mathrm{Bi_{eff}}$ – Biot number based on the effective thermal conductivity:

$$\mathrm{Bi_{eff}} = \frac{\mathrm{hL}}{\mathrm{Keff}} \tag{23}$$

The dimensionless boundary and initial conditions are the same reported in model 1, but in addiction the following conditions need to be considered, for the cold blow:

$$\begin{aligned} &\frac{\partial \vartheta_s}{\partial x^*}(t^*, 0) = 0 \\ &\frac{\partial \vartheta_s}{\partial x^*}(t^*, 1) = 0 \end{aligned} \tag{24}$$

for the hot blow:

$$\begin{aligned} &\frac{\partial \vartheta_s}{\partial x^*}(t^*, 0) = 0 \\ &\frac{\partial \vartheta_s}{\partial x^*}(t^*, 1) = 0 \end{aligned} \tag{25}$$

for the magnetization/demagnetization process:

$$\begin{aligned} &\frac{\partial \vartheta_s}{\partial x^*}(t^*, 0) = 0 \\ &\frac{\partial \vartheta_s}{\partial x^*}(t^*, 1) = 0 \end{aligned} \tag{26}$$

3.3. Model with axial conduction in the solid and in the secondary fluid equations (model 3)

$$\begin{cases} (A.K.)_f = A \ \mathrm{L} \ K_{eff,f} \ \dfrac{\partial^2 \mathrm{T_f}}{\partial \mathrm{x}^2} \\ (A.K.)_s = A \ \mathrm{L} \ K_{eff,s} \ \dfrac{\partial^2 \mathrm{T_s}}{\partial \mathrm{x}^2} \end{cases} \tag{27}$$

In the present study, the dispersion phenomenon is treated as an additional diffusive term added to the stagnant component [41]. The stagnant component is expressed in terms of phase porosities and the individual thermal conductivities of the phases. The empirical correlation developed by Wakao and Kaguei [30] is employed in this study to model the effective conductivities [42].

$$\begin{aligned} K_{eff,f} &= \varepsilon \quad \mathrm{k_f} + 0.5 \left[\mathrm{Pr}_f \left(\frac{\rho_f \ \mathrm{w_f} \ \mathrm{d_p}}{\mu_f} \right) \right] \mathrm{k_f} \\ K_{eff,s} &= (1-\varepsilon) \quad \mathrm{k_s} \end{aligned} \tag{28}$$

The axial conduction terms in dimensionless form are:

$$\begin{cases} (\mathrm{A.K.})_{\mathrm{f,dl}} = \dfrac{1}{\mathrm{Pe_f}} \dfrac{\partial^2 \vartheta_\mathrm{f}}{\partial \mathrm{x}^{*2}} \\ (\mathrm{A.K.})_{\mathrm{s,dl}} = \dfrac{\mathrm{St_f}}{\mathrm{Bi_s}} \Phi \dfrac{\partial^2 \theta_s}{\partial \mathrm{x}^{*2}} \end{cases} \tag{29}$$

Where the following dimensionless numbers have been used:

- $\mathrm{Pe_f}$ – fluid Peclet number:

$$\mathrm{Pe_f} = \mathrm{RePr} \tag{30}$$

- $\mathrm{Bi_s}$ – Biot number based on the effective thermal conductivity of the magnetic material:

$$Bi_s = \frac{hL}{K_{eff,s}} \tag{31}$$

The dimensionless boundary and initial conditions are the same reported in model 3, but in addiction, the following conditions need to be considered, for the cold blow:

Int. J. Energy Res. 2013; **37**:1475–1487 © 2012 John Wiley & Sons, Ltd.
DOI: 10.1002/er

$$\frac{\partial \vartheta_f}{\partial x^*}(t^*, 0) = 0 \tag{32}$$

for the hot blow:

$$\frac{\partial \vartheta_f}{\partial x^*}(t^*, 0) = 0 \tag{33}$$

for the magnetization/demagnetization process:

$$\begin{aligned} \frac{\partial \vartheta_f}{\partial x^*}(t^*, 1) &= 0 \\ \frac{\partial \vartheta_f}{\partial x^*}(t^*, 0) &= 0 \end{aligned} \tag{34}$$

4. NUMERICAL SOLUTION

There is not analytical solution to solve for the equations presented previously. The numerical solution for the fluid and regenerator temperatures is obtained over a grid that extends from 0 to 1 in dimensionless space and from 0 to total dimensionless cycle time in time. The computer program used to numerically solve the equations is Mathematica [43].

The Runge–Kutta explicit method has been used to solve the equations system. In this simulation, a fourth stage stepping scheme has been adopted for the numerical solution, with a discretization of 50 steps in time and space integration.

Because the model concerns a thermodynamic cycle, the following condition has to be respected:

$$\vartheta_s(0, x^*) = \vartheta_s(1, x^*) \tag{35}$$

An iterative resolution of equation (6) provides the regime solution utilizing a tentative profile of the dimensionless temperature of the magnetic bed. The calculative cycle stops when the error δ reported below is smaller than $1*10^{-6}$:

$$\delta = \mathrm{Max}\{|\vartheta_s(0, x^*) - \vartheta_s(1, x^*)|\} \tag{36}$$

The dimensionless refrigeration energy and energy supplied to the environment are calculated according to the following equations:

$$Q^*_{ref} = \frac{Q_{ref}}{\dot{m}_f \bar{C}_f \tau (T_h - T_c)} = -\int_{t_D^*}^{t_D^* + t_{CF}^*} \vartheta_f \, dt^* \tag{37}$$

$$Q^*_{rej} = \frac{Q_{rej}}{\dot{m}_f \bar{C}_f \tau (T_h - T_c)} = \int_{t_D^* + t_{CF}^* + t_M^*}^{t_D^* + t_{CF}^* + t_M^* + t_{HF}^*} \vartheta_f \, dt^* \tag{38}$$

The second law coefficient of performance is valuable as:

$$\xi_{II} = \frac{COP}{COP_{MCI}} = \frac{COP}{\frac{T_c}{T_h - T_c}} \tag{39}$$

5. RESULTS AND DISCUSSION

In the simulation, the temperature ranges that have been explored are 260 – 280 K and 275 – 295 K. These ranges correspond to typical domestic refrigeration temperatures.

The heat transfer mediums are, respectively, water–glycol mixture (50% by weight) and pure water. The $Gd_{0.8}Dy_{0.2}$ alloy and pure Gd have been chosen as constituent materials for the regenerator of the AMR cycle. Indeed, the Curie temperature of pure Gd is out of 260–280 K temperature range, whereas the Curie temperature of the $Gd_{0.8}Dy_{0.2}$ alloy (corresponding to 269 K) is in the middle.

The regenerator in this simulation has a cylindrical geometry and is comprised of packed spheres of magnetic material.

In this simulation, a NdFeB permanent magnet is used in Halbach configuration with a field generation of 1.5 T.

In this analysis, the influence of the main working parameters on cycle performances has been studied by means of the dimensionless numbers.

The first parameter that has been analysed is the diameter of the magnetic refrigerant. Varying this diameter, the porosity of the bed also varies. For spheres packed in cylindrical tube, this effect can be estimated by the following equation [44]:

$$\varepsilon = 0.78\left(\frac{d_p}{D}\right)^2 + 0.375 \tag{40}$$

In this analysis, the variation of porosity with the particle diameters was negligible.

At a fixed aspect ratio (L/D), the mean values of the utilization factor ϕ was constant while the number of heat transfer units varies, increasing with the decrease of the diameter of the spheres of magnetic solid.

In the temperature span range 260 – 280 K, with $Gd_{0.8}Dy_{0.2}$ as magnetic material and water–glycol mixture as secondary fluid, the mean value of Φ is 0.208.

The numerical analysis has been developed for each dimensionless model, one model that neglects the axial conduction effect (Model 1) and two models that take into account this effect (Model 2 and Model 3).

Figure 3 reports the second law coefficient of performance ξ_{II} as a function of NTU.

Figure 3 displays that for each model, the ξ_{II} coefficient first increases with NTU reaching a maximum and after decreases. Indeed, the heat transfer area per unit length increases decreasing the particle diameter, increasing the cooling power. On the other end, the resistance to the fluid flow also increases increasing the work of the pump. ξ_{II} presents a maximum; therefore, there exists an optimal NTU values for each constant Φ that maximize the energetic performance of the cycle. This maximum corresponds to a low value of NTU (around 111) because water–glycol is a very viscous fluid and therefore the effect of the increase of the work of the pump prevails.

The figure clearly shows that the three models give comparable results in term of energetic performances of the cycle except that for NTU values lower than 200. It should be noted that convective heat transfer is extremely important to consider at low particle diameter (corresponding to high NTU) and thus dominate the heat transfer of the fluid. On the other hand, axial conduction is extremely important to consider at high particle diameter (corresponding to low NTU). Under these conditions, the convective heat transfer

is of the same order as the axial conduction, and therefore it is not possible to neglect the conduction terms in the energy balance.

In the temperature span range 275 – 295 K, with Gd as magnetic material and water as secondary fluid, the mean Φ value is 0.2706. Figure 4 reports the second law coefficient of performance ξ_{II} as a function of NTU. In this temperature range, the maximum of the efficiency corresponds to a higher value of NTU (around 410) because water is a less viscous fluid. The three models give comparable results in term of energetic performances of the cycle except that for NTU values lower than 400.

The second parameter that has been investigated is the fluid blow time. A variation of the later parameter corresponds to a variation of the frequency of the pump motor speed. In the simulation, the secondary fluid mass flow rate was held constant; therefore, NTU remains constant while Φ varies.

Figure 5 shows ξ_{II} values varying Φ in the temperature span range 260–280 K, corresponding to a NTU value of 103. The figure clearly shows that increasing Φ, ξ_{II} decreases. Indeed, increasing the fluid blow time (and therefore Φ), the mass of water–glycol flowing in the bed increases, increasing the work of the pump. The three models give comparable results in terms of energetic performances of the cycle for Φ values greater than 0.27. At high fluid blow time (corresponding to high Φ values), convective boiling dominates heat transfer. On the other hand, the thermal conduction is extremely important at low fluid blow time where the three models give different results. The conduction losses decrease the refrigerant power and therefore the energetic performance of the cycle.

Figure 6 shows the ξ_{II} values varying Φ in the temperature span range 275–295 K corresponding to a NTU value of 262. This figure clearly shows that ξ_{II} increases with Φ reaching a maximum (around 0.4) and afterward decreases. The rise of refrigerating power with the mass of the fluid improves the energetic performances. When the increase of the pump work prevails on the rise of the refrigeration power, the energetic performances decrease. Therefore, using water as a secondary fluid, there is a Φ values that maximizes the ξ_{II} coefficient at constant NTU. The three models give comparable results in terms of energetic performances of the cycle for Φ values greater than 0.49.

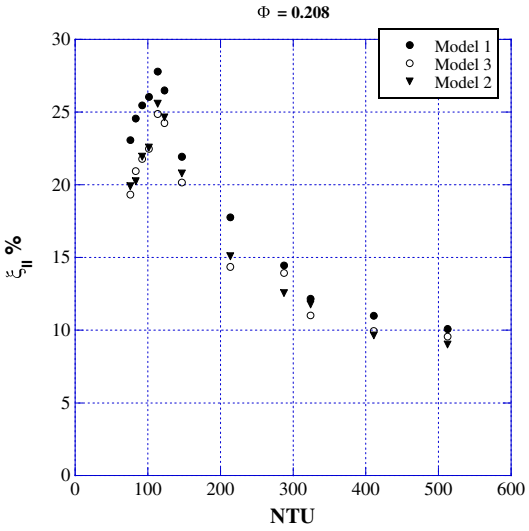

Figure 3. The effect of magnetic material particle diameter: ξ_{II} as a function of NTU at a ϕ value of 0.208 in 260 – 280 K temperature range with water–glycol as a secondary fluid.

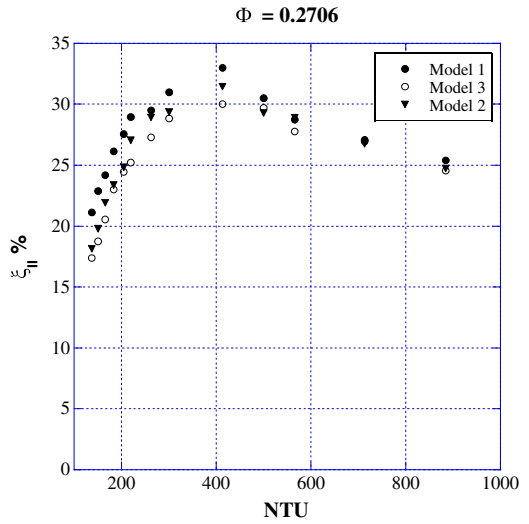

Figure 4. The effect of magnetic material particle diameter: ξ_{II} as a function of NTU at a ϕ value is 0.2706 in 275– 295 K temperature range with water as a secondary fluid.

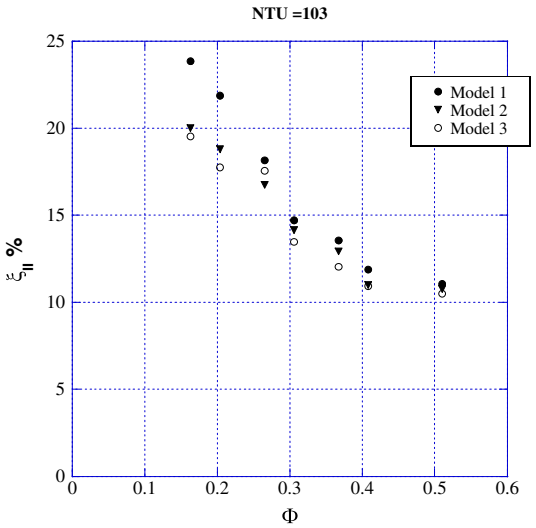

Figure 5. The effect of the fluid blow time: ξ_{II} as a function of ϕ at NTU = 103, in the temperature span range 260–280 K with water–glycol as a secondary fluid.

Int. J. Energy Res. 2013; **37**:1475–1487 © 2012 John Wiley & Sons, Ltd.
DOI: 10.1002/er

The third parameter is the mass of the secondary fluid. Increasing the latter, Φ increases and NTU decreases.

Figure 7 reports the ξ_{II} values as a function of Φ and NTU in the 260–280 K temperature range. The figure shows that ξ_{II} decreases with the increase of the secondary fluid mass flow rate. Increasing the latter parameter, the pressure drops, and therefore the work of the pump strongly increases.

The three models show comparable results in the high secondary fluid mass flow rates and different results in the low. It should be noted that the thermal conduction is important to consider at low mass flow rates (Φ lower than 0.47 and NTU greater than 129) whereas at high mass flow rate convection dominates heat transfer.

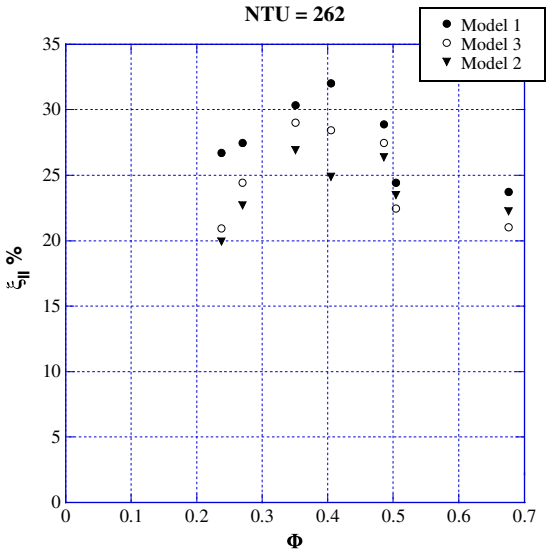

Figure 6. The effect of the fluid blow time: ξ_{II} as a function of ϕ at NTU = 262, in the temperature span range 275–295 K with water as a secondary fluid.

Figure 8 reports the ξ_{II} values as a function of Φ and NTU in the 275–295 K temperature range. ξ_{II} increases with water mass flow rate reaching a maximum and afterward decreases. The rise of refrigerating power with the secondary fluid mass flow rate improves the energetic performances. When the increase of the work of the pump prevails, the energetic performances decrease. Therefore, using water as a secondary fluid, there are a Φ and NTU values that maximize the ξ_{II} coefficient. The three models give different results for Φ values greater than 0.54 and NTU lower than 260.

The effect of regenerator geometry at a given volume has been investigated by choosing a total regenerator volume and varying the aspect ratio (L/D) in 260 – 280 K temperature range. Increasing the aspect ratio at constant volume, NTU increases at fixed Φ. The regenerator's cross-sectional area decreases, and therefore the secondary fluid velocity at constant mass flow rate increases, thus increasing the heat transfer coefficient and therefore NTU.

The investigation has been carried out with four different regenerator's volumes corresponding to four different Φ values (0.175, 0.218, 0.283, 0.410). Figure 9 shows that the three models give different results for NTU lower than a 130, while, for values greater than 130, the results are comparable. The ξ_{II} coefficients of the model 1 always decrease increasing NTU at fixed Φ. Indeed, increasing NTU, the regenerator length and therefore the pressure drops also increase. Both models 2 and 3 show first an increase and after a decrease of ξ_{II} with NTU. ξ_{II} presents a maximum; therefore, there exists an optimal NTU for a given Φ that

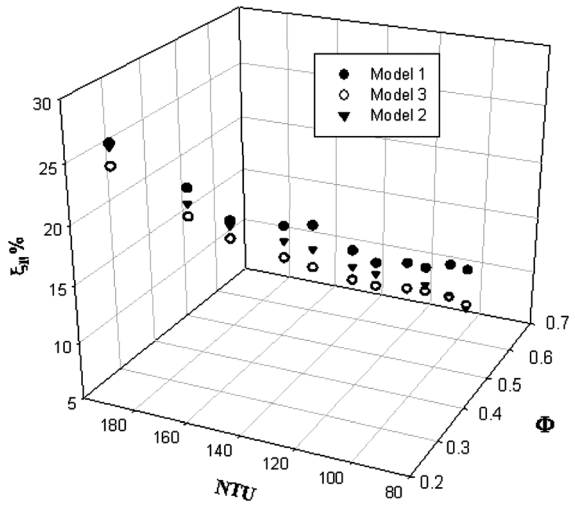

Figure 7. The effect of secondary fluid mass flow rate: ξ_{II} as a function of ϕ and NTU in the temperature span range 260–280 K with water–glycol as a secondary fluid.

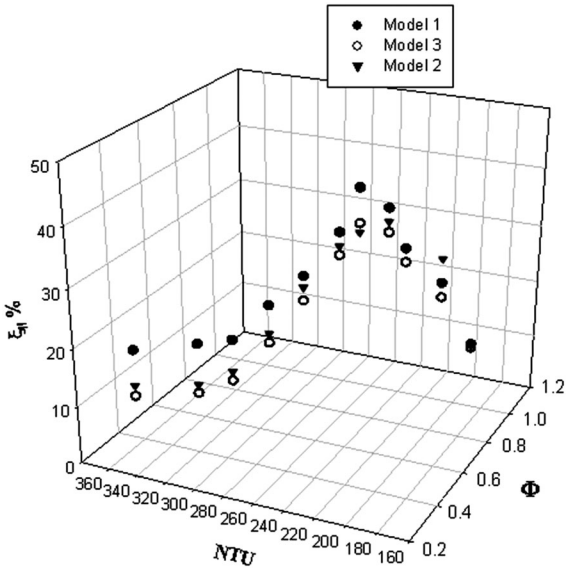

Figure 8. The effect of secondary fluid mass flow rate: ξ_{II} as a function of ϕ and NTU in the temperature span range 275–295 K with water as a secondary fluid.

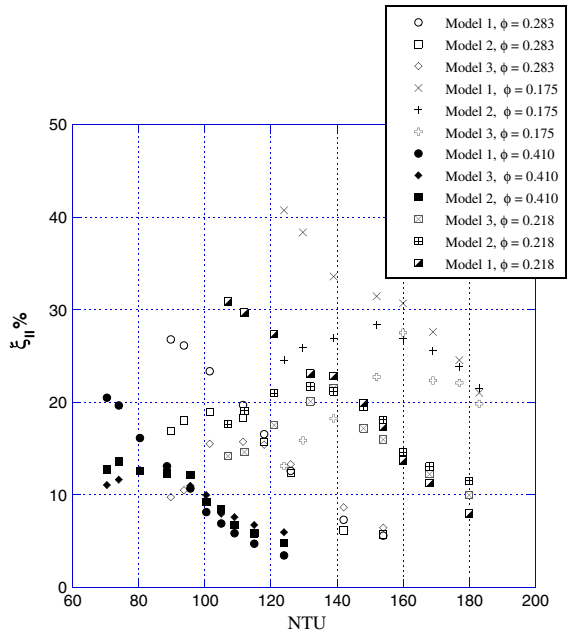

Figure 9. The effect of regenerator geometry: ξ_{II} as a function of NTU for different ϕ values in the temperature span range 260–280 K with water–glycol as a secondary fluid.

corresponds to the higher energetic performance of the cycle. Indeed, lower NTU values result excessive conduction losses, whereas higher NTU result excessive pumping losses. The model with no axial conduction term over predict cycle performance in the lower NTU range because is not able to predict the heat conduction losses. Therefore, the latter model cannot individuate the optimal NTU, which provides the maximum ξ_{II} corresponding to any fixed Φ.

This figure also shows that for each model decreasing Φ (at fixed NTU), the energetic performances of the cycle always increase. Indeed, increasing the regenerator's volume (and thus decreasing Φ), the magnetic material mass also increases increasing the MCE and therefore the cycle performances.

6. CONCLUSIONS

Several numeric models were discussed for the simulation of AMR cycles. The results, however, are rather specific and cannot be extended to different regenerators or different working conditions. The model proposed in this paper was set up in dimensionless form, thus enabling the extension of the results to widely different situations. Furthermore, it can be applied to the design of an experimental prototype in which the set of operational parameters are such as to achieve optimal energetic performance.

In the simulation, the temperature range that has been explored is 260 – 280 K and 275 – 295 K. The heat transfer mediums are, respectively, water–glycol mixture (50% by weight) and pure water. The $Gd_{0.8}Dy_{0.2}$ alloy and pure Gd have been chosen as constituent material for the regenerator of the AMR cycle.

With this model, the influence of the different dimensionless numbers on cycle efficiency has been analysed. In particular, the study has been focused on the influence of the secondary fluid properties, magnetic material particle diameter, fluid blow time, secondary fluid mass flow rate, regenerator geometry and effect of axial thermal conduction.

Based on simulations, it is possible to draw the following conclusions:

1. **Effect of secondary fluid on cycle performances**: The viscosity of the water–monoethylenglycol mixture (50% by weight) is greater than that pertaining to pure water. The effect of the greater viscosity of the secondary fluid is an increase of pressure drops. Therefore, with the mixture, the work of the pump has a great influence on cycle performances. For this secondary fluid, in order to maximize the energetic performances of the cycle, it is better to use magnetic material particle of large diameters (corresponding to low NTU at fixed Φ), low fluid blow time (corresponding to low Φ at fixed NTU), low mass flow rate (corresponding to high NTU at low Φ) and high values of regenerator's volume (corresponding to low Φ at fixed NTU). Using water as a secondary fluid, the effect of the work of the pump on cycle performances is less marked, and there are optimal values that maximize cycle performance of particle diameters (corresponding to NTU at fixed Φ), fluid blow time (corresponding to Φ at fixed NTU), fluid mass flow rate (corresponding to NTU and Φ) and regenerator's volume (corresponding to low Φ at fixed NTU).
2. **Effect of magnetic material particle diameter on cycle performances**: Varying this parameter, the mean values of the utilization factor Φ were constant, while the number of heat transfer units varies. The energetic performances of the cycle first increase with NTU reaching a maximum and afterward decrease. Therefore, there exist optimal NTU values for each constant Φ that balance the effect of the increase of the cooling power and of the increase of the work of the pump.
3. **Effect of magnetic fluid blow time on cycle performances**: Varying this parameter, the NTU remains constant, while Φ varies. Increasing this parameter, both the refrigerating power and the work of the pump increase. When the increase of the pump work prevails, the energetic performances decrease. If the secondary fluid is water, there is an optimal value of Φ that maximizes the performance of the cycle.
4. **Effect of secondary fluid mass flow rate on cycle performances**: Varying this parameter, both NTU and Φ vary. Increasing this parameter, both the refrigerating power and the work of the pump increase. When the increase of the pump work prevails, the energetic performances decreases. If the secondary fluid is water, there is an optimal value of Φ and NTU that maximizes the performance of the cycle.

Int. J. Energy Res. 2013; **37**:1475–1487 © 2012 John Wiley & Sons, Ltd.
DOI: 10.1002/er

5. **Effect of regenerator's volume on cycle performances**: Varying this parameter at constant aspect ratio, Φ varies at fixed NTU. Increasing the regenerator's volume (and thus decreasing Φ), the magnetic material mass also increases increasing the magnetocaloric effect and therefore the cycle performances.
6. **Effect of the regenerator's shape on cycle performances**: Varying this parameter at constant volume, NTU varies at fixed Φ. Increasing NTU, the energetic performance of the plant first increases and afterward decreases. Therefore, there exist optimal values of NTU that maximize the cycle performance balancing conduction and pumping losses.
7. **Effect of axial conduction on cycle performances**: The influence of this parameter depends on the regenerator's shape and on the operating conditions. The effect of conduction losses is always a decrease of the energetic performances of the cycle. This effect cannot be neglected for regenerators characterized by a low aspect ratios (low NTU) and/or for small values of utilization factors Φ.

NOMENCLATURE

Symbols

A	= heat transfer surface, m^2
B	= magnetic induction, Tesla T
C	= specific heat, J/kgK
$\bar{C}$	= mean value of specific heat, J/kgK
COP	= coefficient of performance of a refrigerator
D	= diameter of the regenerator section, m
D_t	= dispersion term
d_p	= diameter of the particles, μm
fo	= function in Hadley correlation
h	= heat transfer coefficient, W/m^2K
H	= magnetic field strength, A/m
k	= thermal conductivity, W/mK
Keff	= effective thermal conductivity, W/mK
L	= length of the regenerator, m
Mn	= magnetization, A/m
m	= mass, kg
$\dot{m}$	= mass flow rate, kg/s
p	= pressure, Pa
P	= secondary fluid flow blow time, s
Q	= thermal energy, J
S	= entropy, J/K
s	= specific entropy, J/kgK
T	= temperature, K
t	= time, s
v	= specific volume, m^3/kg
V	= volume, m^3
W	= work, J
w	= local velocity, m/s
x	= space, m
x_m	= mass fraction

Dimensionless numbers

Bi_{eff}	= Biot number based on the effective thermal conductivity
Bi_s	= Biot number based on the solid thermal conductivity
Φ	= utilization factor
Φ^o	= utilization factor with no fluid flow
H*	= dimensionless magnetic field
x*	= dimensionless space
NTU	= number of transfer units
NTU^o	= number of transfer units with no fluid flow
p*	= dimensionless pressure
Pe	= Peclet number
Pr	= Prandtl number
Q*	= dimensionless thermal energy
Re	= Reynolds number
St_f	= fluid Stanton number
S_H	= dimensionless magnetic material number
θ	= dimensionless temperature
t*	= dimensionless time

Greek symbols

αo	= function in Hadley correlation
Δ	= finite difference
ε	= porosity
ξ_{II}	= second law coefficient of performance
μ	= viscosity, Pa s
ρ	= density, kg/m^3
τ	= reference time, s

Subscripts

ad	= adiabatic
B	= magnetic field constant
c	= cold
CF	= cold water flow
D	= demagnetization phase
dl	= dimensionless
f	= fluid
h	= hot
H	= magnetic field constant
HF	= hot water flow
inf	= undisturbed flow
M	= magnetization phase
m	= magnetic
max	= maximum
M.C.I.	= Inverse Carnot Machine
min	= minimum
p	= particle
p	= pump
ref	= refrigeration
rej	= reject
sc	= effective heat transfer
s	= solid
T	= constant temperature
tot	= total

REFERENCES

1. Zimm C, Jastrab A, Stenberg A, Pecharsky VK, Gschneidner KA Jr, Osborne M, Rohsenow WM, Hartnett JP, Ganic ENI. *Handbook of Heat Transfer*. McGraw-Hill: New York, NY, 1985; chapter 6, 10–11.
2. Yu BF, Gao Q, Zhang B, Meng XZ, Chen Z. Review on research of room temperature magnetic refrigeration. *International Journal of Refrigeration* 2003; **26**:622–636.
3. Landymore K. Electrical Energy Reduction in Refrigeration and air Conditioning, Report. Smartcool System Inc., 2007.
4. Calm JM. Emissions and environmental impacts from air-conditioning and refrigeration systems. *International Journal of Refrigeration* 2002; **25**:293–305.
5. Annual Energy Review 2010. Report DOE/EIA-0384 (2010). US Department of Energy, USA, October 2011.
6. Pecharsky VK, Gschneiner KA. Magnetoaloric effect and magnetic refrigeration. *Journal of Magnetism and Magnetic Materials* 1999; **200**:44–56.
7. Kim S, Ghirlanda S, Adams C, Bethala B, Sambandam S, Bhansali S. Design, fabrication and thermal design of a magnetocaloric mocrocooler. *International Journal of Energy Research* 2007; **31**(6–7):717–727.
8. Gschneidner K, Pecharsky VK. Thirty years of near room temperature magnetic cooling: where we are today and future prospects. *International Journal of Refrigeration* 2008; **31**:945–961.
9. Yu B, Liu M, Egolf PW, Kitanovski A. A review of magnetic refrigerator and heat pump prototypes built before the year 2010. *International Journal of Refrigeration* 2010; **33**:1029–1060.
10. Nielsen KK, Tusek J, Engelbrecht K, Schopfer S, Kitanovski A, Bahl CRH, Smith A, Pryds N, Poredos A. Review on numerical modelling of active magnetic regenerators for room temperature applications. *International Journal of Refrigeration* 2011; **34**:603–616.
11. Petersen TF, Engelbrecht K, Bahl C, Elmegaard B, Pryds N, Smith A. Comparison between a 1D and a 2D numerical model of an active magnetic regenerative refrigerator. *Journal of Physics D: Applied Physics* 2008; **41**:105002–105010.
12. Bjørk R, Bahl CRH, Smith A, Pryds N. On the optimal magnet design for magnetic refrigeration. *The 3rd International Conference of IIR on Magnetic Refrigeration at Room Temperature*, Des Moines, USA, 11–15 May 2009.
13. Kitanovski A, Diebold M, Vuarnoz D, Gonin C, Egolf PW. Application of magnetic refrigeration and its assessment. Final report for the Swiss Federal Office of Energy, 2008; 1–40.
14. Bjørk R, Bahl CRH, Smith A, Pryds N. Review and comparison of magnet designs for magnetic refrigeration. *International Journal of Refrigeration* 2010; **33**:437–448.
15. Bjørk R, Smith A, Bahl CRH. Analysis of the magnetic field, force, and torque for two-dimensional Halbach cylinders. *Journal of Magnetism and Magnetic Materials* 2010; **322**:131–141.
16. Bjørk R, Bahl CRH, Smith A, Christensen DV, Pryds N. An optimized magnet for magnetic refrigeration. *Journal of Magnetism and Magnetic Materials* 2010; **322**:3324–3328.
17. Bjørk R, Bahl CRH, Smith A, Pryds N. Comparison of adjustable permanent magnetic field sources. *Journal of Magnetism and Magnetic Materials* 2010; **322**: 3664–3671.
18. Gopal BR, Chahine R, Földeaki M, Bose TK. Non-contact thermoacustic method to measure the magnetocaloric effect. *The Review of Scientific Instruments* 1995; **66**:232–238.
19. Gschneidner KA Jr, Percharsky VK. The influence of magnetic field on thermal properties of solids. *Materials Science and Engineering* 2000; **287**:301–310.
20. Dai W, Shen BG, Li DX, Gao ZX. New magnetic refrigeration materials for temperature range from 165 K to 235 K. *J. Alloys Compounds* 2000; **311**:22–27.
21. Barclay JA. The theory of an active magnetic regenerative refrigerator. *NASA STI/Recon Technical Report N* 1982; **83**:34087.
22. Aprea C, Greco A, Maiorino A. A numerical analysis of an active magnetic regenerative cascade system. *3rd International Conference on Magnetic Refrigeration at Room Temperature, IIR Conference*, Des Moines, United States, May 11–15, 2009.
23. Aprea C, Greco A, Maiorino A. A numerical analysis of an Active Magnetic Regenerative Cascade system. *International Journal of Energy Research* 2011; **35**:177–188.
24. Aprea C, Greco A, Maiorino A, Tura A. Numerical analysis of an Active Magnetic Regenerative Refrigeration cycle with a Gd-Dy multi-layer regenerator. *Proceedings of ASME-ATI-UIT 2010 Conference on Thermal and Environmental Issues in Energy Systems*, Sorrento, Italy, 16 – 19 May 2010.
25. Aprea C, Greco A, Maiorino A. A numerical analysis of an Active Magnetic Regenerative Refrigerant system with a multi-layer regenerator. *Energy Conversion and Management* 2011; **52**:97–107.
26. Amiri A, Vafai K. Transient analysis of incrompressible flow through a packed bed. *International Journal of Heat and Mass Transfer* 1998; **41**:4259–4279.
27. Pei-Xue J, Ze-pei R, Bu-Xuan W. Numerical simulation of forced convention heat transfer in porous plate

channels using thermal equilibrium and nonthermal equilibrium models. *Numerical Heat Transfer Part A* 1999; **35**:99–113.
28. Klein H, Eigenberger G. Approximate solutions for metallic regenerative heat exchangers. *International Journal of Heat and Mass Transfer* 2001; **44**:3553–3563.
29. Nellis GF, Klein SA. Regenerative heat exchangers with significant entrained fluid heat capacity. *International Journal of Heat and Mass Transfer* 2006; **49**:329–340.
30. Wakao N, Kaguei S, Funazkri T. Effect of fluid dispersion coefficients on particle-to-fluid heat transfer coefficients in pace beds. *Chemical Engineering Science* 1979; **34**:325–336.
31. Wakao N, Kaguei S. *Heat and Mass Transfer in Packed Beds*. Gordon and Breach: New York, 1982.
32. Kaviany M. *Principles of Heat Transfer in Porous Media*. Springer: New York, NY, 1995; 33, 46–47, 130, 228–229.
33. Sarlah A, Poredos A. Dimensionless numerical model for simulation of active magnetic regenerator refrigerator. *International Journal of Refrigeration* 2010; **33**:1061–1067.
34. Tishin AM, Spichkin YI. *The magnetocaloric effect and its applications*. Institute of Physics Publishing: Bristol and Philadelphia, 2003; 13–14.
35. Bingfeng Y, Zhang Y, Qiang G, Dexi Y. Research on performance of regenerative room temperature magnetic refrigeration cycle. *International Journal of Refrigeration* 2006; **29**:1348–1357.
36. Balli M, Allab F, Dupuis C, Fruchart D, Gignoux D, Kedous-Lebouc A, Fournier JM, Yonnet JP. Analysis and modelling of magnetocaloric effect near magnetic phase transition temperature, *Second IIF-IIR International Conference on Magnetic Refrigeration at Room Temperature*, Portozm Slovenia, 11–13 April 2007.
37. Balli M, Fruchart D, Gignoux D, Miraglia S, Hlil EK, Wolfers P. Modelling of the magnetocaloric effect in Gd1-xTbx and MnAs compounds. *Journal of Magnetism and Magnetic Materials* 2007; **316**:558–561.
38. Bean CP, Rodbell DS. *Physics Review* 1961; **126**:104.
39. Rodbell DS. *Physical Review Letters* 1961; **7**:1.
40. Hadley GR. Thermal conductivity of Packed Metal Powders. *International Journal of Heat and Mass Transfer* 1986; **29**(6):909–919.
41. Hunt ML, Tien CL. Non-Darcian convention in cylindrical pace beds. *Journal of Heat Transfer* 1988; **110**:378–384.
42. Feng Y, Yu B, Zou M, Zhang D. A generalized model for the effective thermal conductivity of porous media based on self-similarity. *Journal of Physics D: Applied Physics* 2004; **37**:3030–3040.
43. Wolfram Mathematica 8. Wolfram Research 2011.
44. Achenbach E. Heat flow characterstics of packed beds. *Experimental Thermal and Fluid Science* 1995; **10**:17–27.